

A Dynamical Study of Optically Selected Distant Clusters

Richard G. Bower,¹ F. J. Castander,² Warrick J. Couch,³ R. S. Ellis² and H. Böhringer⁴

¹ *Dept. of Physics, University of Durham, South Road, Durham, DH1 3LE, U. K.*
² *Institute of Astronomy, Cambridge University, Madingley Road, Cambridge, CB3 0HA, U. K.*
³ *School of Physics, University of New South Wales, NSW 2052, Australia*
⁴ *Max Planck Institut für Extraterrestrische Physik, 85740 Garching, München, Germany*

ABSTRACT

We present a programme of spectroscopic observations of galaxies in a sample of optically-selected clusters taken from the catalogue of Couch et al (1991). Previous ROSAT observations of these clusters have shown them to have lower X-ray luminosities, given their optical richness, than might be expected on the basis of local samples. In the present paper we extend this work by determining velocity dispersions of a subsample of the clusters. We confirm the dynamical reality of all but one of the original sample, and find velocity dispersions comparable with present-day clusters of equivalent comoving space density. Thus, in the context of the $L_X - \sigma$ relation for present-day clusters, there is evidence for a higher velocity dispersion at fixed X-ray luminosity.

A key question is whether the high velocity dispersions are indicative of the gravitational potential. If they are, the X-ray luminosities measured in Bower et al., 1994 (Paper I), would then imply an implausibly low efficiency of X-ray generation. Alternatively, the discrepancy could be explained if the clusters were systems of lower virial temperature, in which the apparent velocity dispersion is inflated by an infalling, unrelaxed halo. By co-adding our sample, we are able to consider multi-component fits to the velocity distribution and to demonstrate evidence for a large infalling population. This might result either from an increase with redshift in the infall rate for clusters, or from the preferential selection of clusters embedded in filaments oriented along the line of sight. Since clusters with similar properties can be found in local optically selected catalogues, we suggest that the latter explanation is more likely.

1 INTRODUCTION

This work is based on the catalogue of optically-selected distant clusters compiled by Couch et al., 1991 (CEMM). Clusters were selected purely on the basis of the over-density of faint galaxies on contrast enhanced AAT 4-m photographic plates. The selection was not implemented by computer algorithm, but objectivity was tested exhaustively using simulations. The total area of sky searched was 46 deg². Clusters with a density enhancement more than 4σ above the local background were then selected for spectroscopic observation in order to determine their redshifts. The redshift of a cluster was only accepted when two or more galaxies with consistent galaxies were found.

Bower et al. (1994, here after Paper I) first used this catalogue to study the X-ray evolution of clusters. A subset of 14 clusters were targeted in pointed ROSAT observations. The clusters were found to have surprisingly low X-ray luminosities, indeed several were not detected at all despite exposure times in excess of 14 ksec. It was shown that this result could be explained by mild negative evolution of the X-ray luminosity function of the type suggested by Henry

et al. (1992) on the basis of the initial EMSS survey. Similar results have been found in other surveys based on optical selection criterion (eg., Nichol et al., 1994, Holden et al., 1997), although the most recent X-ray selected surveys conflict over the extent of the evolution they find (eg., Castander et al., 1995, Rosati et al., 1995, Nichol et al., 1997, Collins et al., 1997).

In this paper, we present a dynamical study of the CEMM cluster sample. Initially, the data will be used to confirm the physical existence of the clusters that we have targeted. The cluster members will then be used to investigate the velocity structure of the clusters. In particular, we will compare the velocity dispersion with the cluster X-ray luminosities presented in Paper I, using the present-day X-ray luminosity – velocity dispersion ($L_X - \sigma$) correlation as a guide. There are three physical regimes we can consider. Firstly, if the evolution of the clusters is driven primarily by the evolution of their gravitational structure, we should expect their velocity dispersions to be smaller than those of present-day clusters of equivalent luminosity (eg., Kaiser, 1991). Secondly, evolutionary models in which the entropy of the cluster gas is a dominant factor predict that the evo-

lution of cluster luminosities and velocity dispersions will be parallel each other so that little evolution of the L_X - σ is expected (Henry & Evrard, 1991). The third possibility is that the velocity dispersions are higher than can be explained by the models discussed above. Such a situation could result if the dynamical state of the clusters was dominated by infall and/or merging. In this case, the velocity dispersion would no longer be representative of the virial temperature of the cluster (eg., Frenk et al., 1990).

As we will show in the following sections, it is difficult to obtain redshifts for large samples of galaxies in these clusters, and we must consider how many redshifts are necessary to determine an adequate estimate of the velocity dispersion. In an isolated cluster, a sample of 10 cluster members, are relatively accurate measurement can, theoretically, be obtained. For example, a measured dispersion of 600 km s^{-1} might arise from a system with true velocity dispersion of between 498 km s^{-1} and 812 km s^{-1} at the 1σ (68%) confidence level. This accuracy is adequate to distinguish between massive and poor clusters (eg., Zabludoff et al., 1993). To obtain better definition, we would have to substantially increase the number of measured redshifts. In practice, however, although adding further members increases the measurement precision only slowly, it greatly reduces the sensitivity of the estimated velocity dispersion to inclusion or exclusion of outlying galaxies. Unfortunately it is extremely inefficient to increase the size of datasets for the clusters individually, so we address this problem by combining the individual clusters to create a single synthetic system: sufficient data are then available to robustly estimate the average dispersion. Furthermore, two component fitting can be used to investigate whether the clusters can be separated into a virialised core and higher dispersion infalling halo.

The outline of the paper is as follows. Section 2 sets out the data on which this paper is based. Specifically, Section 2.1 summarises the X-ray data from Paper I and presents data for the additional cluster F1557.19TC ($z = 0.51$), while Section 2.2 describes the spectroscopic data that are central to this study. The analysis of the cluster redshift distributions is detailed in Section 3, including our analysis of the combined dataset. In Section 4, we discuss the implications of the high dispersions that we find, including a comparison with evolutionary models. Our conclusions are presented in Section 5.

2 DATA REDUCTION

2.1 X-ray Data

The clusters studied in this paper were selected from the CEMM clusters for which we had obtained pointed ROSAT PSPC observations, the seven clusters being chosen in such a way as to optimise the efficiency of the spectroscopic observing programme.

The X-ray data for these systems have for the most part been presented in Paper I. The exception is the cluster F1557.19TC, for which the data were not presented because its redshift of 0.51 exceeds the completeness limit that we set in the earlier paper. The X-ray data for F1557.19TC were reduced in identical manner to that used in Paper I. To summarise, we measure the total (ie., cluster plus background) flux falling within a $3' \times 3'$ detect cell centred on the optical

Table 1. X-Ray Properties of the Cluster Sample

Cluster	Redshift	N_H^1	Exposure ²	Cts ³	Backgr ⁴	Luminosity ⁵
F1557.19TC	0.51	4.0	21.03	36.	94.	0.477
F1652.20CR	0.41	3.2	15.10	34.	66.	0.395
F1637.23TL	0.48	1.1	23.98	48. †	39.	0.487
J2175.15TR	0.41	1.4	11.50	45.	26.	0.647
J2175.23C	0.40	1.4	19.77	20.	53.	0.156
F1835.22CR	0.469	3.9	21.30	19. †	42.	0.225
F1835.2CL	0.377	3.9	17.20	-8. †	37.	< 0.142

Notes:

- ¹ Hydrogen column density towards cluster in units of 10^{20} atoms cm^{-2} .
- ² Exposure time in ksec, corrected for telescope vignetting.
- ³ Photon count in detection cell after background subtraction. Where marked †, the photon count is measured in channels 52–201, otherwise in channels 41–240. For pointed data, a detect cell size of $3' \times 3'$ has been used; All Sky Survey data uses a larger detect cell ($4' \times 4'$) to allow for the wider point-spread function.
- ⁴ Background count rate determined from spline fit (pointed observations) or mean of surrounding area (All Sky Survey observations).
- ⁵ Cluster luminosity in the 0.7–3.5 KeV (in the cluster rest-frame) in units of 10^{44} erg s^{-1} . A factor of 0.7 is included in order to allow for the flux that is lost from the detected cell. Where the cluster is not detected with greater than 99% confidence, the flux corresponding to the 99% detection threshold is given.

position of the cluster. The flux was then compared with the background flux measured from a background spline fit. Where the excess flux in the cluster detect cell did not exceed the 99% confidence detection threshold (determined by the shot noise in the background within the detect cell), the detection threshold is quoted as an upper limit. The X-ray flux derived in this way has been converted to rest-frame luminosity assuming a cluster temperature of 5 keV (throughout the paper, we adopt the cosmological parameters $H_0 = 50 \text{ km s}^{-1} \text{ Mpc}^{-1}$ and $q_0 = 0.5$). The cluster luminosities are presented in Table 1.

Due to an error in Paper I, the X-ray luminosities given there were incorrectly quoted as referring to the cluster rest-frame 0.5–2.5 keV energy band. In actuality, the table gave luminosities in the observed-frame energy band. For consistency, the data in Table 1 have been referenced to the 0.7–3.5 keV energy band in the cluster rest-frame. For a cluster with redshift 0.40, the two energy bands are equivalent. Small differences from the values presented in Table 1 of Paper I occur when the actual redshift of the cluster is taken into account. Correcting the error in Paper I shifts the best fitting luminosity function by -0.15 in $\log(\text{luminosity})$, further increasing the significance of the result presented there.

2.2 Spectroscopic Data

Spectroscopic observations were undertaken to considerably supplement the redshift data obtained for the clusters by CEMM. The observations were made with the 3.6m telescope at the European Southern Observatory, La Silla, using the high throughput EFOSC grism spectrograph

(D’Odorico, 1990, Melnick, 1991). The data were gathered during two observing runs in January and December, 1994: the clusters F1835.22CR, F1835.2CL and J2175.23C being targeted during the first run; F1557.19TC, F1652.20CR, F1637.23TL and J2175.15TR in the second. Both runs used the same instrumental set-up, the O150 Grism (and Tektronix CCD #26) providing a dispersion of 3.6\AA per pixel and an empirical resolution of 10\AA (FWHM).

In order to achieve our target of at least 10 members in each cluster, we observed each cluster twice using multi-object masks created with the PUMA punching machine. This enabled 24 objects to be observed in, at most, a $3.6'$ diameter field. In practice, almost all of the cluster members were drawn from within 0.5 Mpc of the cluster centre given by CEMM. With the aim of reducing field contamination, we attempted to preferentially select red objects for observation (using colours estimated from the original photographic plates and short exposure CCD frames), but found that the constraints of requiring both wavelength coverage from at least 3600\AA to 4500\AA in the cluster rest frame (which determines the acceptable range of spatial offsets from the masks center), and a minimum slit length of $10''$ allowed relatively little freedom in the choice of objects.

The redshifts measured from our EFOSC (1994) spectra are given in Table 2, and typical spectra are illustrated in Figure 1. For absorption-line galaxies, redshifts were measured by overlaying a high signal-to-noise template spectrum constructed by co-adding the spectra of the brighter objects. The redshift determination could then be made by sliding the template spectrum in redshift until the strong features matched those in the target galaxy. By offsetting the template, the accuracy of the redshift measurement could be judged. As a result of the high dispersion and oversampling of the spectra, we found that once the target spectrum showed convincing absorption features, its redshift could be determined to better than 0.001. For a galaxy cluster at redshift 0.4, this corresponds to a velocity resolution of 214 km s^{-1} in the cluster rest-frame. In order to avoid confusion by residuals from the background subtraction, a night sky spectrum was also overlaid in this fitting process. In some of the clusters, this is very important because one of the strong Ca H and K lines can be obliterated by the night sky emission feature at 5577\AA .

For emission line galaxies, the redshift was measured by centroiding the emission feature. Where both absorption and emission features were present, the two methods agreed to better than $\Delta z = 0.001$. In a number of cases, only one emission line and no discernible absorption features were present. Since the emission line was narrow, we assumed this was [OII] at 3727\AA . These redshifts are marked in Table 2 to indicate this uncertainty. For the purposes of measuring the velocity dispersion of the cluster, the ambiguity of these measurements is unimportant since it principally involves field galaxies at redshifts significantly higher or lower than the cluster. Mis-identification of the emission line is most unlikely to result in the false assignment of a field galaxy to the cluster.

Galaxies with emission-line equivalent width greater than 7\AA are noted in Table 2. This division is used to investigate the dependence of the measured velocity dispersion on star formation rate in Section 3.

Finally, we returned to the longslit spectra obtained by

CEMM (where available) to provide redshifts for an additional 2–3 cluster members in each system. As CEMM required the redshifts only to establish cluster membership, we considered it necessary to re-reduce the spectra and re-measure the galaxy redshifts. Revised redshifts were determined using the techniques and templates discussed above, with the sky spectra from the two data sets being monitored to check the consistency of the data reduction. The reworked redshifts are given in Table 3. In the few cases where the measurements differ, our more precise measurements are to be preferred.

3 RESULTS

3.1 Redshift Distribution Histograms

Figures 2(a–g) and 3(a–f) present the velocity histograms for each cluster. Two views are given, one showing the distribution on a coarse scale (Figure 2a–g), the second focusing on a rest-frame velocity range of $\pm 4000\text{ km s}^{-1}$ about the cluster mean (Figure 3a–f). F1835.2CL is not shown in Figure 3 because of the lack of any single galaxy concentration. The first point we conclude from these figures is that, in all but one case, the cluster (although identified from its two dimensional projection on the sky) corresponds to a genuine physically associated system: the selection of the cluster by CEMM as a two dimensional density enhancement is confirmed as a sharp spike in redshift space in our data. The exception to this is the cluster F1835.2CL, for which the 12 galaxies that could be measured returned only one redshift close to the cluster redshift proposed by CEMM.

The small-scale panels allow us to visually assess the cluster velocity dispersions. It can immediately be appreciated that while a velocity dispersion can be readily calculated from these galaxies, it is very much more difficult to be certain that this value is representative of the gravitational potential of the cluster. There are essentially two kinds of contamination that are liable to affect our results. Firstly, the cluster may actually be composed of two (or more) distinct gravitational components. Hopefully, such a situation would be apparent from the double-peaked nature of the small-scale redshift distribution. If the velocity separation of the cluster components is small, however, the small sample of redshifts available to us is unlikely to show a statistically significant effect. It seems unlikely, however, that this problem would equally affect all of the clusters. Secondly, individual outliers such as close-by field galaxies may appear close to the cluster in redshift space and thus artificially inflate the measured dispersion. This possibility must be countered by applying a variety of clipping algorithms to the data and testing the robustness of the dispersions that we find.

3.2 Measuring the Cluster Velocity Dispersion

The velocity dispersions of the clusters are given in Table 4. Four values are quoted to illustrate different approaches determining the central value and the effect of excluding emission-line galaxies. All values are quoted in km s^{-1} and have been transformed to the cluster rest-frame. The velocity dispersion is defined as $\sum_{i=1}^n (v_i - \bar{v})^2 / (n - n_{df})$, where n is the number of galaxies in the sample, n_{df} is the

Table 2. New Spectroscopic Redshifts

Table 2a. F1557.19TC				Table 2b. F1652.20CR				Table 2c. F1637.23TL									
Obj	z	Obj	z	Obj	z	Obj	z	Obj	z	Obj	z						
A2	0.245	e	B2	0.539	A1	0.353	e	B1	0.353	e	A1	0.466	B5	0.478			
A4	M star		B5	0.507	A2	0.409		B3	0.411		A2	0.654	e†	B6	0.482	e†	
A5	0.539	e	B6	0.508	A3	0.411		B4	0.077	e	A3	0.465		B10	0.402	e	
A6	0.509		B9	0.510	A4	0.410		B5	0.212	e†	A4	0.537	e†	B12	0.478		
A7	0.185	e	B13	0.426	e	A5	0.406	e†	B6	0.420		A5	0.655	e	B14	0.475	
A8	0.507				A6	0.411	e†	B9	0.217		A8	0.482		B15	0.344	e†	
A9	0.517				A7	0.255	e				A9	0.536					
A10	0.509				A8	0.417					A14	0.479					
A11	0.512	e†			A9	0.409					A15	0.810	e†				
A12	M star				A11	0.478					A16	0.475	e†				
					A12	0.218	e				A19	M star					
					A14	0.482	e										
					A15	0.411	e										
					A16	M star											

Table 2d. J2175.15TR				Table 2e. J2175.23C				Table 2f. F1835.22CR								
Obj	z	Obj	z	Obj	z	Obj	z	Obj	z	Obj	z					
A2	0.395		B1	0.332	e	A2b	0.354	e	B1	0.393		A1	M star	B1	0.240	e
A3	0.553		B5	M star		A3	0.402		B2	0.151	e	A3	M star	B3	0.473	e
A4	0.553		B7	0.394		A4	0.402	e†	B3	0.402		A4	0.468	B6	0.500	
A5	0.418	e†	B8	0.395		A5	0.453	e	B4	0.386	e†	A5	0.471	B10	0.715	e†
A6	0.167	e	B10	0.400		A6b	0.373	e†	B5	0.535	e†	A6	M star	B11	0.321	e
A7	0.397		B12	0.331	e	A7	0.396	e†	B9	M star		A7b	0.470			
A9	0.362	e				A8b	0.408		B11	0.596		A9	0.472	e		
A10	0.395					A11	0.406		B12a	0.5	e†	A10	0.478			
A11	0.394								B12b	—		A11	0.186			
A12	0.392								B13	0.471	e†	A12	0.466			
A13	0.337	e														

Table 2g. F1835.2CL				
Obj	z	Obj	z	
A1a	0.442	B7	0.302	e
A2	0.477	B8	0.486	e
A3	0.442			
A4	0.212	e		
A6a	0.444	e		
A7	0.303			
A8	0.315			
A9b	0.377			
A10b	0.415			

Notes:

e Spectrum contains emission lines with greater than 7\AA equivalent width.

† Redshift is based on only one line.

number of degrees of freedom that have been absorbed in defining the cluster mean. For a single cluster, $n_{df} = 1$, for the composite cluster (see Section 3.3) $n_{df} = n_{clus}$, where n_{clus} is the number of clusters being used to make up the composite. This definition of the dispersion compensates for bias that arises when we use the galaxy sample to determine the mean cluster redshift. We refer to this value as ‘the cluster dispersion’ in what follows.

We chose *a priori* to give most weight to the estimate

based on iterative 3σ clipping starting from a high nominal dispersion of 1500 km s^{-1} (Method 1). This scheme is preferred since the clipping corresponds to a natural division of cluster and background galaxies, and the high initial dispersion ensures that a wide range of data is initially considered before outliers are selected and rejected. The final result is insensitive to both the assumed value of the dispersion and the initial mean value. Monte-Carlo simulations were performed to confirm that the clipping resulted in negligible

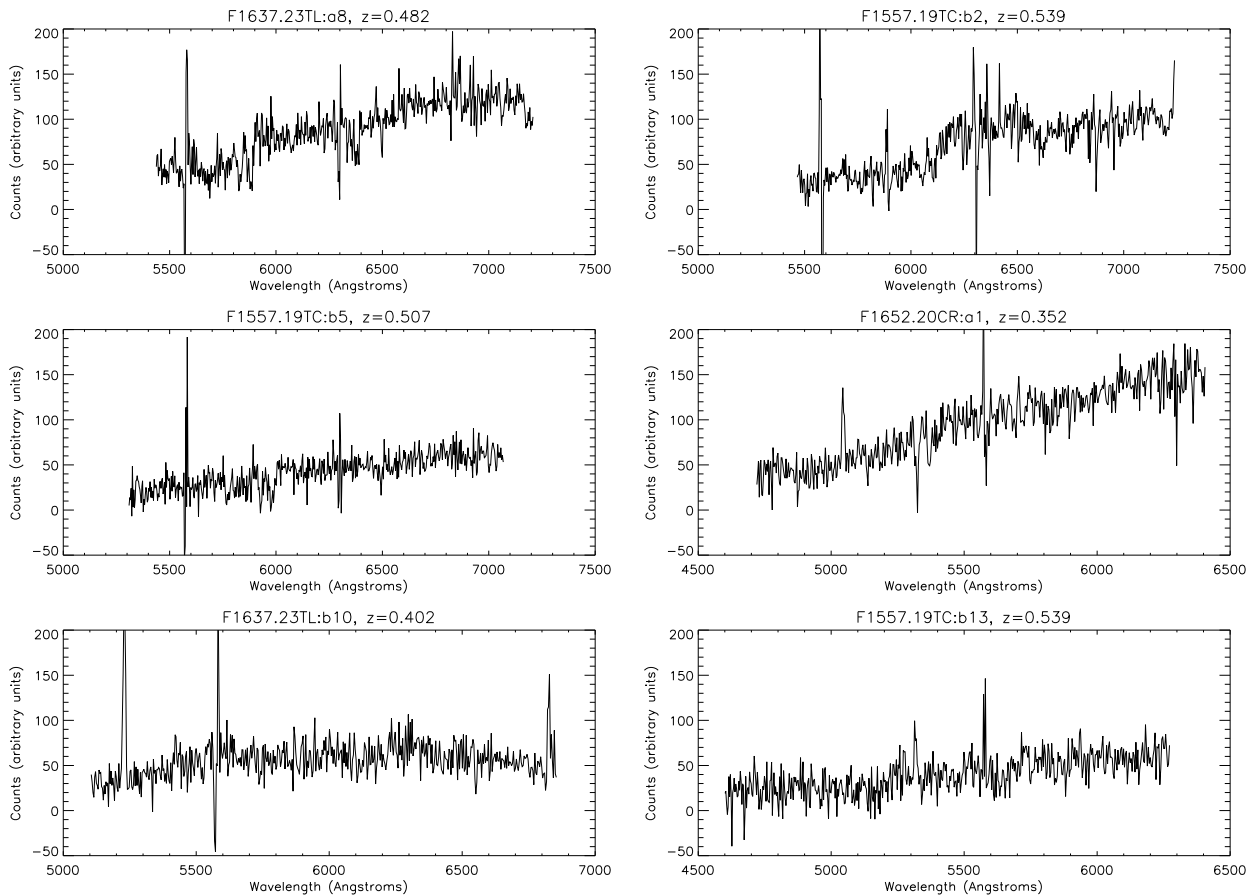


Figure 1. Examples of typical spectra taken with the EFOSC system. These are raw spectra, and the residuals remaining for subtraction of strong night-sky emission lines can be clearly seen. The plots are labelled with the object code given in Table 2.

Table 3. Revised Redshifts for CEMM Spectra

Cluster	Obj	z	comment
F1557.19TC	a	0.509	
	c	0.509	
F1652.20CR	<i>CEMM spectra not available</i>		
F1637.23TL	1	0.479	
	4	0.465	OII emission
	5	0.482	
J2175.15TR	a	0.396	
	d	0.406:	
	j	—	
J2175.23C	a	0.405	
	b	0.407	
	c	0.406	
F1835.22CR	<i>CEMM spectra not available</i>		

bias in the measured dispersion. Furthermore, the scatter in the values derived from the simulations agreed well with those expected on the basis of the F-ratio test (eg., Kendall & Stewart, 1973). F-ratio 68% confidence limits for the estimated cluster dispersions are therefore given in columns

5 and 6 of Table 4. The measured (sample) dispersions for the cluster data are over-plotted on the small scale view of Figure 3. In order to assess whether a single Gaussian distribution provides an acceptable fit to the data, and thus to test whether there is any detectable substructure within the clusters, we performed Kolmogorov-Smirnoff (KS) tests on the unbinned velocity values. Because of the small numbers of objects involved, the data must be folded about the cluster mean (ie., on the values of $|v_i - \bar{v}|$). The resulting confidence of acceptance is given in Table 4. In none of the clusters is the departure significant.

As can be seen from the table, this approach returns relatively high values for the dispersion. The model Gaussian distribution is shown as a continuous line in Figure 3. Visual inspection of the figure suggests that the distribution is more centrally peaked than the Gaussian curve in the three clusters F1557.19TC, F1652.20CR and J2175.15TR. If the clusters are taken individually, this kurtosis is not flagged by the KS distribution test; however, the qualitative impression is that of a halo of galaxies surrounding a much lower dispersion central core. The only cluster that suggests a binary structure (ie., being composed of two distinct velocity peaks) is F1637.23TL, but again this is not flagged by the KS test.

Another approach to determining the velocity dispersion is to use the median to determine the central cluster redshift, and then to perform the clipping about this value.

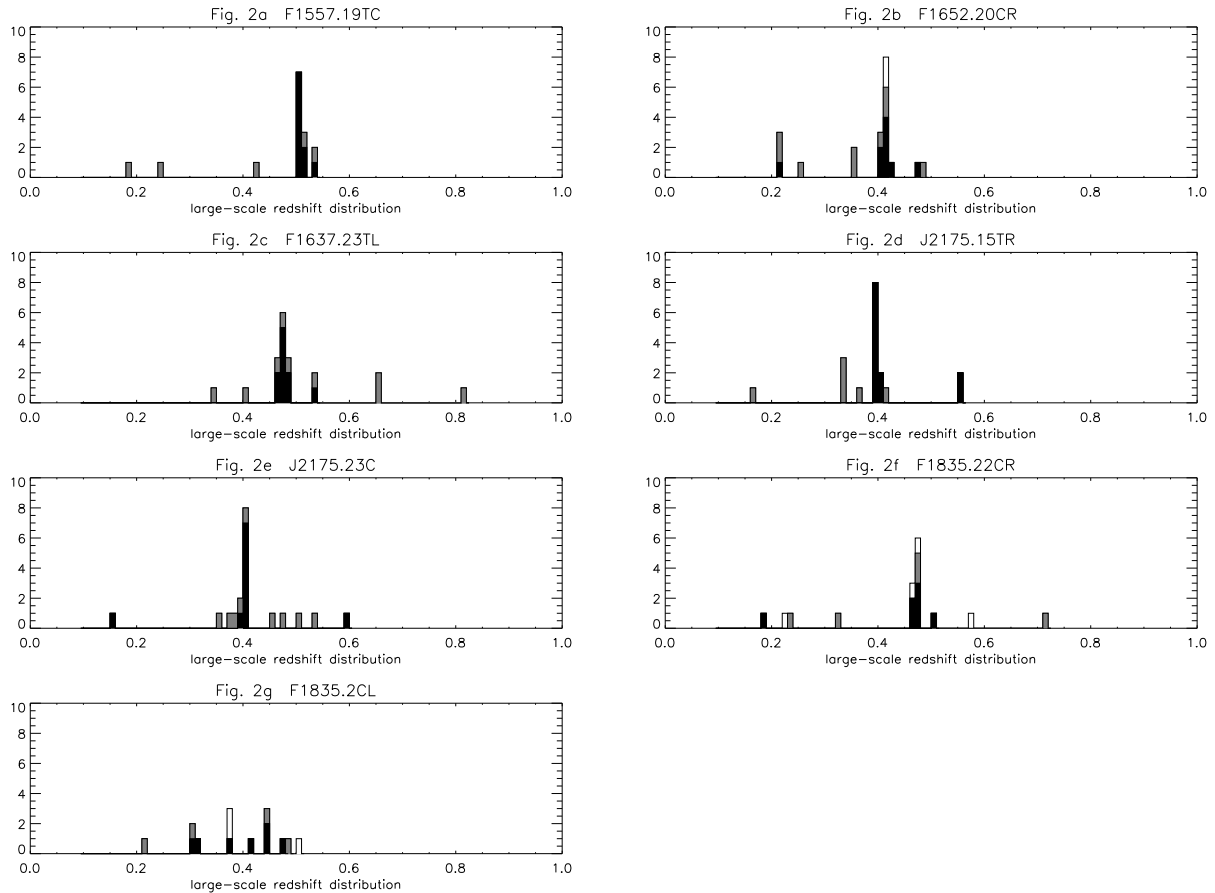


Figure 2(a–g). The large-scale redshift distribution of all objects for which velocities have been measured. The shading identifies the different galaxy types: solid, absorption line galaxies; half-tone, emission line objects. Redshifts taken from CEMM’s paper but which were unavailable for re-reduction are left unshaded. In all but the case of F1835.2CL, there is a single clear density peak in redshift space.

This makes it more likely that outlying points will be rejected since they have less influence on the choice of cluster centre. The actual effect on the cluster dispersions is, however, minimal. We were also concerned that the inclusion of strong emission line galaxies to determine the cluster dispersion might lead to artificially high values. This was tested by repeating the analysis for the low emission line equivalent width galaxies only. Once again, there was little change from the dispersion measured using all the available galaxies.

In order to make a quantitative assessment of the impact of outlying points, we experimented with a variety of more stringent clipping algorithms. As can be seen from Table 4, clipping the velocities used in the calculation of the dispersion at 2σ has a significant effect on the clusters F1557.19TC and J2175.15TR. In these clusters, this experiment confirms the visual impression that the velocity distribution is more centrally concentrated than would be expected for a Gaussian distribution (ie., the distribution is leptokurtic). In order to investigate the effect further, however, we must co-add the data for the individual clusters. This approach is discussed in Section 3.4.

3.3 The L_X - σ Correlation

Figure 4 compares the X-ray luminosities of the CEMM

clusters with their line-of-sight rest-frame velocity dispersion. Data for the individual clusters are shown as open diamond symbols. The velocity data used are the 3σ clipped and bias corrected values discussed above. The error bars show the 68% F-test confidence interval for the dispersion. For comparison, a fiducial data-set has been taken from Edge & Stewart (1991, ES) (with luminosities and temperatures updated from David et al., 1993) These data are shown as crosses in Figure 4. This dataset differs from that of CEMM in including both nearby clusters and those sampled on the basis of X-ray flux. We have transformed the nearby clusters to the 0.7–3.5 keV band using the given cluster temperatures and assuming an iron abundance of 0.33 solar. The best fitting present-day L_X - σ correlation is given by the thin line, with its uncertainty indicated by the shaded region.

Although the scatter in the relation for ES clusters is large, the velocity dispersions of our distant clusters lie clearly above the mean correlation defined by the fiducial data-set. What cannot be determined from this diagram alone, however, is whether the CEMM clusters are lower in their X-ray luminosity, or higher in their velocity dispersion.

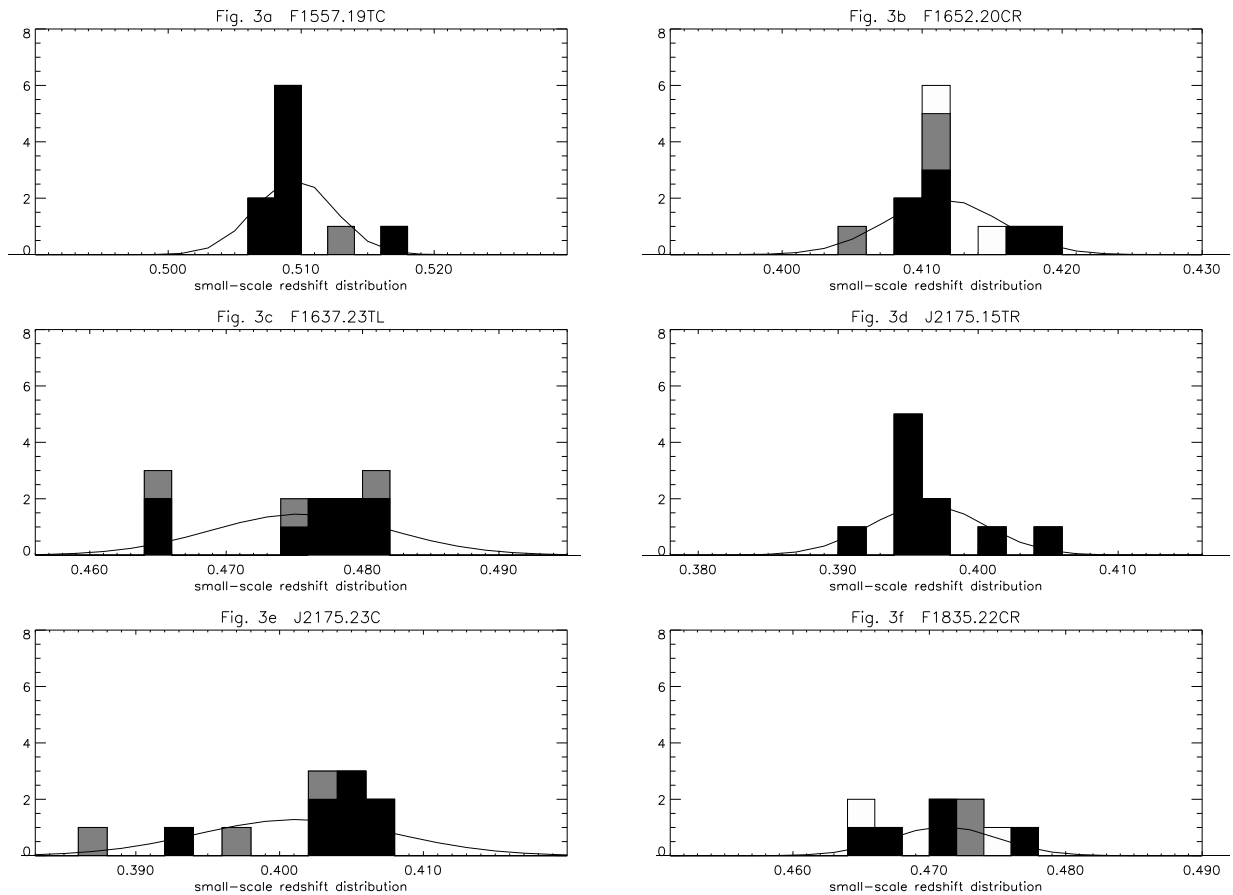


Figure 3(a–f). The small scale redshift distribution centered on each of the bona-fide CEMM clusters. The shading of the histogram distinguishes the object types as in Figure 2. The Gaussian distribution overlaid shows the Method 1 fit given in Table 4. All plots have been scaled to show a range of $\pm 4000 \text{ km s}^{-1}$ (in the cluster rest-frame) about the mean cluster redshift.

3.4 Analysis of a Composite Cluster

The dispersion measured for each individual cluster has a large statistical uncertainty. For example, the cluster J2175.15TR is compatible at the 1σ level with dispersions ranging from 707 to 1156 km s^{-1} . Thus a quantitative comparison with present-day clusters must be made by combining the separate clusters. This may be achieved by averaging the results for the individual systems, or by merging the galaxy velocities to create a composite velocity distribution for the entire sample. The advantage of combining our data in the second way is that outlying points, or a non-Gaussian tail to the velocity distribution, should become more visible. Of course, in combining the data in this way, two assumptions are implicit. Firstly, the clusters must have similar velocity dispersions. Secondly, the systems must be assumed not to be binary (ie., composed of two distinct systems aligned along the line of sight): if this were the case, co-adding the individual systems would tend to obscure any substructure in the velocity distribution.

In order to combine the clusters, galaxy redshifts were converted to rest-frame velocity offsets about the centre of target cluster (as given in Table 3). These were then transformed back to create a synthetic redshift distribution for a cluster with redshift 0.45 (Figure 5). We repeated the proce-

dure using the median, rather than mean, to re-centralise the different clusters prior to co-addition in order to investigate the composite’s sensitivity to outliers. Velocity dispersions were measured using iterative 3σ clipping, and a number of other schemes, as described in Section 3.2. The results are given at the end of Table 4. The measured velocity dispersion (derived using 3σ clipping) is $930 \binom{1033}{852}$, significantly higher (at more than 99.9% confidence) than the average value of the present-day L_X – σ correlation. This data-point is illustrated by a solid circle in Figure 4.

In order to guard against the inclusion of binary clusters, the dispersion was recalculated omitting the cluster F1637.23TL. This is the only cluster for which the velocity dispersion histogram gives a visual impression of binary structure. Although this structure is of low statistical significance, omitting this cluster tests the robustness of the final dispersion. As can be seen from the Table 4, excluding the cluster slightly lowers the velocity dispersion of the composite dataset (shown as a shaded circle in Figure 4), but the dataset is still inconsistent with the fiducial present-day relation at 99.5% confidence. However, we must be wary of how to interpret this result: the CEMM clusters have been selected from optical imaging, whereas the ES dataset from which we have constructed the present-day relation is derived from an X-ray selected catalogue. We return to this

Table 4. Cluster Velocity Dispersions

Cluster	z	σ_v^a	N	σ_v^{+b}	σ_v^{-b}	P_{KS}^c	Method ^d
F1557.19TC	0.5095	584	10	791	481	0.23	1
	0.5089	355	9	492	291	0.09	2
	0.509	572	10	775	474	0.06	3
	0.5094	597	9	827	490	0.07	4
F1652.20CR	0.4115	863	10	1167	714	0.30	1 [†]
	0.4115	1004	10	1358	831	0.22	2 [†]
	0.411	826	10	1117	683	0.40	3 [†]
	0.4124	916	7	1357	736	0.66	4 [†]
F1637.23TL	0.4755	1335	12	1744	1121	0.80	1
	0.4755	1553	12	2029	1304	0.84	2
	0.478	1373	12	1793	1153	0.17	3
	0.4766	1284	9	1780	1055	0.86	4
J2175.15TR	0.3964	854	10	1156	707	0.52	1
	0.3953	559	9	774	459	0.33	2
	0.395	865	10	1171	716	0.06	3
	0.3969	834	10	1156	707	0.52	4
J2175.23C	0.4012	1463	11	1942	1221	0.84	1
	0.4027	1213	10	1641	1004	0.76	2
	0.402	1405	11	1865	1172	0.33	3
	0.4036	1027	8	1465	835	0.65	4
F1835.22CR	0.4711	784	7	1162	630	0.90	1 [†]
	0.4711	912	7	1351	733	0.71	2 [†]
	0.471	727	7	1076	584	0.89	3 [†]
	0.4706	930	5	1562	723	0.69	4 [†]
F1835.2CL	—	—					
Composite (all clusters)		930	59	1033	852	0.08	1 [†]
		854	54	953	780	0.50*	2 [†]
		907	48	1018	824	0.12	4 [†]
		963	59	1070	833	0.0002	5 [†]
		966	48	1064	860	0.0010	4,5 [†]
Composite (F1637.23TL omitted)		815	47	917	740	0.16	1 [†]
		798	44	901	722	0.05	2 [†]
		916	41	1040	826	0.04	4 [†]
		809	47	911	735	0.009	5 [†]
		829	39	945	747	0.15	4,5 [†]

Notes:

^a Velocity dispersion of cluster members given in km s^{-1} in the cluster restframe.^b 68% upper and lower confidence limits for the velocity dispersion, σ_v , calculated from the F-ratio test. This gives an estimate of the sampling uncertainty in the measured dispersion, but makes no allowance for possible departure of the underlying distribution from Gaussian form.^c Folded KS test probability that galaxies are drawn from a Gaussian distribution with dispersion σ_v . Folding the distribution about the cluster mean increases the test's sensitivity to the kurtosis of the data-set.^d Estimation Methods:

1. 3σ clipping. Initial value of dispersion 1500 km s^{-1} .
2. 2σ clipping. Measured dispersions are corrected by a factor including correction 1.16 to allow for galaxies that are trimmed from the Gaussian tail. Initial value for the dispersion is 1500 km s^{-1} .
3. 3σ clipping about median cluster redshift. Dispersion is calculated without applying a $\sqrt{n/(n-1)}$ bias correction.
4. Method 1 applied to absorption line galaxies only.
5. As method 1, but using median redshift to centralise the galaxy clusters before coaddition.

[†] Velocity dispersion has been calculated excluding unconfirmed CEMM data.

* Centre of fitted gaussian is 0.4509. Although a sharp peak is present in the velocity distribution, this is smoothed out in the folded KS test.

point in Section 4.

In addition to increasing the accuracy of the measured dispersion, the greater size of the composite dataset makes it possible to test the adequacy of the single Gaussian description of the data, and thus to check for an extended tail to the redshift distribution. Firstly, we tested the acceptability

of the fit by applying the Kolmogorov-Smirnoff test to the data folded about the cluster mean. As shown in Table 4, the test rejects the single component fit with confidence levels ranging from 85 to 99.98% depending on how the composite cluster is constructed. Thus, the initial visual impression of a non-Gaussian distribution is confirmed in the larger dataset.

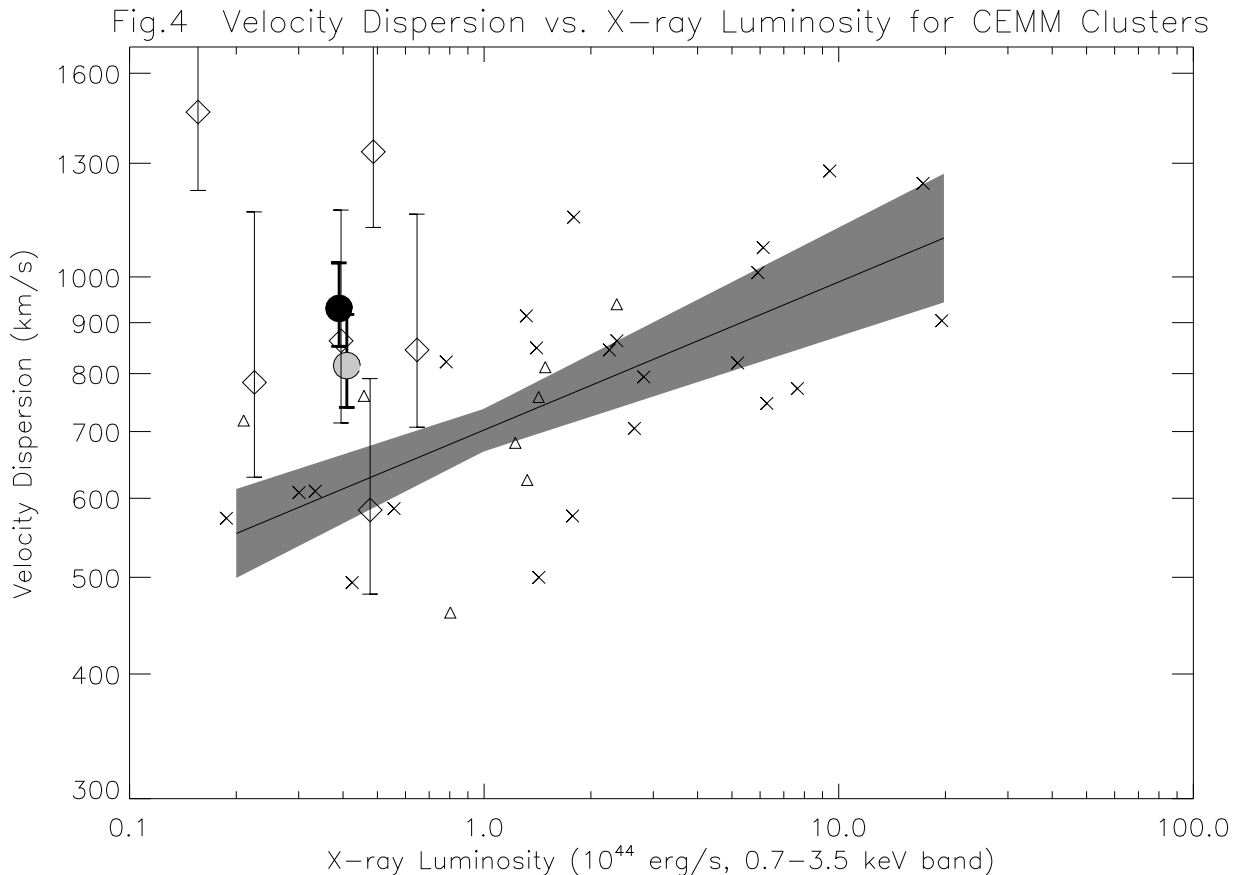


Figure 4. The velocity dispersions and X-ray luminosities of the CEMM clusters (diamonds) compared with the present-day L_X - σ correlation (crosses). The dispersions of the CEMM clusters plotted were determined by applying the iterative 3σ clipping algorithm (Method 1 in Table 4). The position of two versions of the cluster composite are shown: solid circle, all clusters combined; shaded circle, omitting the cluster F1637.23TL. The X-ray luminosity is a simple average over the six individual clusters. The two points have been shifted slightly in X-ray luminosity to improve clarity. The present epoch mean correlation and its uncertainty are shown by the thin line and the shaded region. Open triangles show the position of additional nearby clusters taken from Zabluff et al., 1990.

An alternative method of assessing the deviation from a Gaussian distribution is to apply the maximum likelihood method to fit the data with a two Gaussian components (cf., Ashman et al., 1995). The data were first fit with a single component in order to establish a reference likelihood. The minimisation adjusted both central redshift, dispersion and normalisation. The resulting fit is given in Table 5: the dispersion (1073 km s^{-1}) is similar to that measured by the conventional approach. A second component was then introduced (starting from 500 km s^{-1}) and the minimisation procedure repeated. The new fit resolves the cluster into core and halo components, confirming the visual impression. The best fit dispersions of the components are 1169 km s^{-1} and 177 km s^{-1} : the low dispersion of the core component is striking. This fit is considerably better than the single component version. The likelihood is improved by 10.7 if the clusters are aligned using their mean redshift, or 26.6 if aligned using the median. Interpretation of the absolute statistical significance of these cases depends on the number of degrees of freedom that are associated with the new component (median alignment of the individual clusters, in particular, will always tend to reinforce the impression of a core), and is best addressed by Monte-Carlo simulation.

These show that a likelihood ratio of 11.7 is significant at the 1% level if the clusters are aligned by their mean redshift. If they are aligned using the median, a higher likelihood ratio (20.6) is needed for the same level of significance.

Thus, while the galaxies in the composite cluster have a large velocity dispersion, there is evidence (at the 1% level) to suggest that this may arise from two distinct populations: a low dispersion ‘core’ and a high dispersion ‘halo’. Examining the separate distributions of high and low emission-line equivalent width galaxies suggests that the low dispersion component is present only in the weak-lined population. However, a KS test does not reject the possibility that the two distributions are the same.

Care must be taken not to over-interpret the separation of the composite distribution into ‘core’ and ‘halo’ components. It is clear that the low dispersion component accounts only for a relatively small fraction of the total galaxy population of the cluster: less than 30% of the total population. Therefore, a high velocity dispersion is characteristic of the majority of the cluster galaxies, and is not the result of a few outlying data points. Furthermore, the dispersion of the central component is unreasonably low — it is unresolved in our data — if it is indicative of the clusters’ virial mass. It

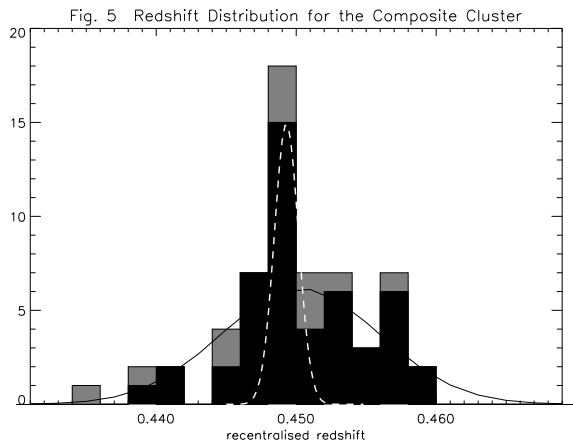


Figure 5. The redshift distribution of the composite cluster formed by co-adding the six individual bona-fide clusters. The velocity offset of each galaxy with respect to its cluster mean has been converted to a redshift offset from a synthetic cluster at $z = 0.45$. Different shadings have been used to distinguish the galaxy spectral types following Figure 2. Gaussian fits derived by applying the iterative 3σ clipping algorithm (Method 1 in Table 4) are showing: dashed line, all galaxies; solid line, absorption line galaxies only.

Table 5. Maximum Likelihood Fits to Composite Distant Cluster

Model Fitted	Galaxy Sample ^a	Central Redshift	σ_v ^b (km s ⁻¹)	Normalisation	Likelihood Ratio ^c
single component	A	0.4498	1073	60.0	
two component	A	0.4503 0.4493	1169 177	43.6 16.1	10.7
single component	B	0.4497	1123	60.0	
two component	B	0.4497 0.4500	1263 88	40.9 19.3	26.6
single component	C	0.4498	896	48.0	
two component	C	0.4504 0.4483	1032 175	34.1 13.9	8.5
single component	D	0.4495	1052	48.2	
two component	D	0.4507 0.4491	1173 217	28.4 19.6	14.8

Notes:

^a Galaxy sample codes: A, all clusters, aligned by mean; B, all clusters, aligned by median; C, all clusters, absorption line galaxies only, aligned by mean; D, as A but omitting F1637.23TL

^b Velocity dispersion is given in km s⁻¹ in the cluster rest frame.

^c Likelihood ratio of two component model versus single component model.

is almost certainly more correct to interpret the core/halo split only as a way of characterising the kurtosis of the velocity distribution, rather than assigning a definite physical significance to the two components.

4 DISCUSSION

In Section 3.3, we showed that the velocity dispersions we measure for these distant clusters lie considerably above that expected on the basis of our fiducial L_X - σ correlation. This departure can be interpreted in one of two ways. The first possibility is that the cluster's X-ray luminosity is low compared to the galaxy velocity dispersion. We could understand this as being due to the evolution of X-ray emission from distant clusters (Paper I). The second possibility is that the discrepancy lies with the velocity dispersion — perhaps a high rate of infall into the distant clusters has caused us to significantly over-estimate the virial temperature. Below, we consider the case for these two interpretations of the data in detail, and investigate the roles played by evolution and the clusters' optical selection.

4.1 Comparison with Nearby Clusters and Models for Cluster Evolution

In order to set an initial expectation of the cluster's velocity dispersion, we use the CEMM cluster space density. This was derived in Paper I from the area of sky covered by the CEMM survey, and the completeness limits of the catalogue. The average density of the clusters relevant to this work is $5 \times 10^{-7} \text{ Mpc}^{-3}$. (We have deliberately avoided making a comparison on the basis of the cluster's apparent richness since (1) our imaging frames are too small to allow an accurate assessment of the background galaxy density, and (2) the apparent richness of the clusters may be substantially affected by changes in the stellar populations of the cluster galaxies — an effect that is discussed extensively in CEMM). Using the velocity dispersion distribution function from Zabludoff et al. (1993), we can convert between the number density of present-day clusters and their expected velocity dispersion. Nearby clusters of the same comoving space-density as the CEMM sample have a characteristic velocity dispersion of $750 (\pm 50) \text{ km s}^{-1}$: in terms of their space density, the clusters are roughly equivalent to Abell clusters at the lower end of richness class 1 (paper 1). We should make it clear that this is the expected average velocity dispersion: the distribution is very strongly skewed to higher dispersions, the tail possibly extending to dispersions as high as 1100 km s^{-1} (adopting a space density a factor of 10 lower for the most extreme cluster).

By contrast, the velocity dispersions that would be inferred from comparison with present-day clusters of comparable X-ray luminosity (ie., $0.4 \times 10^{44} \text{ erg s}^{-1}$ in the 0.7–3.5 keV energy band) are considerably lower. As we have discussed in Section 3, using the L_X - σ correlation from Edge et al. suggests that clusters of the above X-ray luminosity should have velocity dispersions in the range 400 – 700 km s^{-1} (cf., Figure 4), with an average value of 612 km s^{-1} . Thus straightforward comparison with the present-day clusters shows that the average dispersion of the CEMM clusters is comparable with the value predicted on the basis of their space-density but higher than the value expected on the basis of X-ray luminosity.

Such a direct comparison takes no account of the evolution of cluster properties expected between $z = 0.41$ and the present-day. Only if the cosmological density parameter, Ω_0 , is extremely small can we hope to neglect the development of clusters between these epochs. To illustrate the expected

evolution, we consider a family of models in which the universe has critical density (ie., $\Omega_0 = 1$) and the spectrum of density fluctuations can be adequately described by a power-law on the scales relevant to galaxy clusters. For currently popular dark matter models, the power-law index n lies in the range -1 to -1.5 ; we consider $n = -1$ and $n = -2$ as extremes. Under these conditions, scaling relations (dependent on n and an additional parameter that describes the balance between heating and cooling of the intra-cluster medium) can be used to predict the statistical properties of the cluster population at $z = 0.4$ from the observed properties of nearby clusters (eg., Kaiser, 1986, 1991, Evrard & Henry, 1991 [EH], Bower, 1997 [B97]).

Table 6 compares the velocity dispersion of the composite dataset with the L_X - σ correlation predicted in a number of evolutionary models. The evolution of the correlation is calculated using the appropriate scaling, and is then used to convert the average CEMM cluster X-ray luminosity into a predicted velocity dispersion. In the first model, we consider the velocity dispersion expected if both the cluster virial temperature and X-ray luminosity evolve self-similarly (ie., the characteristic densities of the dark matter and the intra-cluster medium [ICM] both remain linked to the background cosmological density). The predicted L_X - σ correlation falls well below the composite CEMM data-point: for clusters of X-ray luminosity as low as is observed for the CEMM systems, the velocity dispersion is predicted to be of order 500 km s^{-1} . Altering the spectral index of fluctuations speeds up the rate of evolution but fails to improve the comparison since the reduction of the model clusters' X-ray luminosities is achieved only at the expense of also lowering the clusters' velocity dispersions.

A greater range of evolutionary scenarios can be generated if we drop the assumption that the ICM follows the same evolution as the dissipationless dark matter component. A promising approach is to assume the intra-cluster gas has constant central entropy (ie., there is no net heating or cooling of the ICM as the cluster evolves). Since the cluster's X-ray luminosity is very sensitive to the central gas density, such a model naturally accounts for the low X-ray luminosities of the clusters. The L_X - σ correlation, however, remains close to its present-day position. Thus, while this model achieves an improvement over the self-similar models discussed above, the discrepancy between the low X-ray luminosities and the high velocity dispersions of the CEMM clusters remains a puzzle. In order to resolve this discrepancy, it is necessary to increase the central entropy of the gas in the distant clusters relative to their present-day counterparts. This can be described through an extension of EH's model that is described in B97: the balance between heating and cooling of the ICM (and thus the evolution of its entropy) is described with an additional parameter, ϵ . The case $\epsilon = 0$ corresponds to EH's original model, while for $\epsilon < 0$ shock heating dominates the evolution of the ICM entropy, and for $\epsilon > 0$ the evolution is dominated by cooling. Closest agreement between the model and the observed properties of the CEMM clusters is obtained by making ϵ positive. However, the cooling rate cannot be made arbitrarily large: the dominant cooling mechanism is X-ray radiation — one of the quantities that we have measured both in the local universe and at high redshift. B97 shows that a conservative upper limit is $\epsilon < 2$. When this constraint is

Table 6. Predicted Velocity Dispersions

Evolutionary Model	Spectral Index (n)	Entropy Parameter (ϵ)	σ_v ^a (km s^{-1})
No Evolution	—	—	612
Self-Similar	-1	(-3)	515
	-2	(-5)	426
Entropy Model	-1	0	579
	-1	+2	625
	-2	0	517
	-2	+2	559

Notes:

^a Mean velocity dispersion predicted for a cluster at redshift 0.41 with $L_X = 0.4 \times 10^{44} \text{ erg s}^{-1}$ in the 0.7–3.5 keV energy band.

included, even this model fails to reproduce the positions of the CEMM clusters in the (L_X, σ) plane, since the evolution of X-ray luminosity and velocity dispersion remain strongly coupled.

4.2 A Non-Virial Interpretation of the CEMM Cluster Velocity Dispersions

The difficulty in providing a theoretical explanation of the position of the single component fit in the L_X - σ plane ensures that we consider alternative interpretations of the high overall dispersion. An artificially high dispersion might arise from (i) a number of distinct, similar sized gravitational units superposed along the line of sight (the dispersion within the individual systems makes them inseparable in redshift space), or (ii) an infalling galaxy population that is bound to the cluster but is not yet virialised (the dispersion of this component is inflated by both the predominance of radial orbits and the physical separation).

In order to address this possibility, we have investigated the robustness of our calculated dispersions to the exclusion of extreme members, and searched for evidence of a non-Gaussian velocity distribution. When the clusters taken individually, there is no statistical evidence of substructure. There is, however, a visual impression of a core-halo structure in many of the clusters (the notable exception being F1637.23TL). Since this is very unlikely to occur by the overlap of physically distinct systems, the infall model is to be preferred.

By stacking all the clusters together, it is possible to quantify the structure of the average velocity distribution. The fit to this composite dataset is indeed improved if a low dispersion centralised component ($\sim 200 \text{ km s}^{-1}$) is added to the high dispersion ($\sim 1000 \text{ km s}^{-1}$) component. The central component contains a minority ($\sim 30\%$) of the cluster galaxies, however, suggesting that it is better to interpret this as evidence for a leptokurtic (strongly peaked) velocity distribution, rather than attaching definite physical significance to the two components. Physically, such a line of sight velocity distribution indicates that a large fraction of the galaxies are moving on radial orbits (eg., Merritt, 1987, Merritt & Tremblay, 1994), a situation that is characteristic

of a cluster that has not yet reached virial equilibrium (ie., in which the galaxies' bulk motion towards the cluster centre dominates over their random motion, Lynden-Bell 1967, Padmanabhan 1993).

One possibility to explain the anomalous dispersion of the CEMM clusters is therefore that these clusters are seen at a period of rapid growth. This picture is appealing since evolution in the dynamical state of clusters might be linked to changes in their galaxy populations (Kauffmann, 1995): specifically, the increased fraction of blue galaxies (eg., Butcher & Oemler, 1978) and the increased proportion of galaxies showing spectral evidence of recent or on-going intense bursts of star formation (eg., Dressler & Gunn, 1983, Couch & Sharples, 1987, Barger et al., 1996). However, another possibility is that the clusters are embedded in large-scale filaments that are oriented along the line of sight. Such systems may have been preferentially selected by the catalogue's optical selection criterion. This effect could boost the apparent infall rate in these systems, making them poorly representative of the distant cluster population as a whole.

In the latter case, we would expect that low redshift optically selected clusters would occupy a similar position in the L_X - σ diagram. To investigate this, we first used clusters from the Zabludoff et al., 1990, survey for which X-ray data was available from the David et al. (1994) compilation. These data points are shown as open triangles in Figure 4. The two lowest X-ray luminosity clusters ($L_X < 0.5 \times 10^{44} \text{ erg s}^{-1}$), indeed lie above our fiducial correlation. Similar results are found for a larger sample of clusters taken from the Edinburgh/Durham Cluster Catalogue (EDCC, Collins et al., 1995, Nichol et al., in prep.). It is not clear whether these data-sets imply a flattening of the L_X - σ correlation at low luminosities or whether averaging over sufficient clusters would produce a mean point lying on the fiducial correlation. Nevertheless, there is clearly evidence for a population of low X-ray luminosity, high velocity dispersion systems at low redshift. These are the nearby counterparts of the CEMM clusters. The existence of such a population in optically selected cluster samples suggests that the selection process cannot be separated from the properties of the resulting cluster population. A connection between the anomalous velocity dispersions and the Butcher-Oemler effect cannot yet be ruled out, however, since we know little about the stellar populations of the galaxies in the nearby systems.

5 CONCLUSIONS

In this paper, we set out to explore the dynamics of a representative sample of galaxy clusters taken from the Couch et al. (1991, CEMM) catalogue. The catalogue identifies clusters as enhancements in the densities of faint objects on deep 4-m optical plates, with initial spectroscopic work being undertaken by CEMM to establishing cluster redshifts on the basis of between 2 and 3 concordant galaxies. Following up this catalogue at X-ray wavelengths, we showed (Bower et al., 1994, Paper I) that the X-ray luminosities of these clusters were well below those of present-day clusters of comparable space density. This is an important result as it reinforces the decline in the amplitude of the X-ray luminosity function of galaxy clusters that is seen in X-ray selected samples (Henry et al., 1992, Castander et al., 1995).

Here, we have undertaken further spectroscopic work in order to increase the number of galaxy redshifts that are available in seven of these clusters. This programme is designed to investigate the dynamics of the clusters and to compare the clusters' velocity dispersions with their X-ray luminosities.

Firstly, however, the study answers a possible criticism of Paper I by establishing the extent to which the optically selected catalogue is contaminated by *projected* galaxy overdensities that result from the superposition of several poor clusters or groups along the line of sight. Such projected associations would not be expected to be X-ray luminous. Typically, we have increased the number of known cluster members to more than 10. In all but one case, the extended redshift survey has confirmed the physical association of the galaxies, a well-defined peak in the redshift distribution being clearly visible.

The main focus of this paper is the velocity distribution of the galaxies in these clusters. This is characterised by the dispersion about the cluster mean. If we make the assumption that these systems are relaxed, it is valid to use the spread of the cluster members' redshifts in order to estimate the depth of the clusters' gravitational potential. Comparison of this with the clusters' X-ray luminosities allows us to investigate the efficiency of the thermal plasma emission in a way that is independent of the cluster's space-density. This approach thus provides an important comparison with the results of Paper I.

We have shown that the clusters' velocity dispersion is high: comparable with that expected on the basis of the clusters' space-density but much higher than would be expected on the basis of the clusters' X-ray luminosity. This conclusion applies whether we consider the clusters individually, or as a composite system.

Relative to the clusters' X-ray luminosities, these dispersions appear to demonstrate that considerable evolution has taken place in the X-ray properties of clusters since $z = 0.4$. However, the strength of the evolution does not match any simple theoretical expectation. The rate of evolution in the X-ray luminosity - virial temperature correlation that is implied cannot be reproduced even within an extreme model of cluster evolution dominated by radiative cooling. Thus although our results seem initially to be in qualitative agreement with observations of a decline in the X-ray luminosities of galaxy clusters, the strength of the effect measured seems unreasonably large.

The lack of a simple explanation for the position of the clusters in the L_X - σ plane forces us to question whether the velocity dispersions we derive can be indicative of the clusters' masses. Closer examination of the velocity histograms of several of the clusters gives an impression that the distribution is excessively peaked compared to a Gaussian, suggesting a core/halo structure. Although this impression is not statistically significant in the individual clusters, it is confirmed at a high level of significance in the analysis of the stacked cluster dataset. The composite cluster is well described by a core component of dispersion $\sim 200 \text{ km s}^{-1}$, and a halo of dispersion $\sim 1000 \text{ km s}^{-1}$. However, the halo component accounts for the larger part of the galaxy population, the core accounting for less than 30% of the total. This suggests that the separate components probably do not have a distinct physical significance; more likely they simply

reflect the peakedness of the velocity distribution.

Our data therefore suggest that the galaxy population of these clusters is dominated by an infalling galaxy halo. We have put forward two possible explanations, one centered on the evolution of clusters, the other resulting from a selection bias. The first interpretation is that these clusters that have not yet formed — or at least are caught at a time of rapid mass growth. The second possibility appears more relevant, however: potentially the clusters selected by CEMM are embedded in large scale structure ‘filaments’ that are being viewed ‘end-on’. Rather than being a consequence of cluster evolution, this could plausibly result from the clusters’ optical selection criterion. This interpretation is given support by the existence of similar low X-ray luminosity - high velocity dispersion systems in optically selected surveys at low redshift. Such an effect might explain the presence of an excess blue galaxy population in some distant clusters, although we would expect the additional galaxies to be drawn from the general field galaxy population rather than being peculiar to the cluster environment. What remains uncertain, however, is whether an evolutionary connection is required: do our results imply an increase in the population of anomalous high dispersion clusters with increasing redshift? Unfortunately, our catalogue is too small and may not adequately sample the full distant cluster population. In order to investigate evolution in optically selected cluster samples, larger cluster catalogues — with matched selection criteria — are needed at both high and low redshift.

ACKNOWLEDGMENTS

We are happy to thank ESO for the provision of the telescope time that made this project possible, and to acknowledge the Starlink project for the provision of computing support. We thank Sharon Lippey for her assistance with the redshift measurements as part of her undergraduate work at the UNSW, and the referee, Bob Nichol, for his helpful comments and suggestions.

REFERENCES

- Ashman, K. M., Bird, C. M., Zepf, S. E., 1995, *AJ*, 108, 2348
 Barger, A. J., Aragon-Salamanca, A., Ellis, R. S., Couch, W. J., Smail, I., Sharples, R. M., 1996, *MNRAS*, 279, 1
 Bower, R. G., 1991, *MNRAS*, 248, 332
 Bower, R. G., 1997, *MNRAS*, in press (B97)
 Bower, R. G., Bohringer, H., Briel, U. G., Ellis, R. S., Castander, F. J., Couch, W. J., 1994, *MNRAS*, 268, 345 (Paper I)
 Butcher, H. R., Oemler, A., 1978, *ApJ*, 219, 18
 Castander, F. J., Bower, R. G., Ellis, R. S., Aragon-Salamanca, A., Mason, O., Hasinger, G., McMahon, R. G., Carrera, F. J., Mittaz, J. P. D., Perez-Fournon, I., Lehto, H. J., 1995, *Nature*, 377, 39.
 Collins, C. A., Guzzo, L., Nichol, R. C., Lumsden, S. L., 1995, *MNRAS* 274, 1071
 Collins, C. A., Burke, D. J., Romer, A. K., Sharples, R. M., Nichol, R. C., *ApJL*, submitted
 Couch, W. J., Sharples, R. M., 1987, *MNRAS*, 229, 423
 Couch, W. J., Ellis, R. S., Malin, D. F., MacLaren, I., 1991, *MNRAS*, 249, 606 (CEMM)
 Couch, W. J., Ellis, R. S., Sharples, R. M. & Smail, I., 1994, *ApJ*, 430, 121
 David, L. P., Slyz, A., Jones, C., Forman, W., Vrtilik, S. D., 1993, *ApJ*, 412, 479

- D’Odorico, S., 1990, EFOSC Observers Manual, ESO Publications
 Dressler, A., Gunn, J. E., 1983, *ApJ*, 220, 7
 Edge, A. C., Stewart, G. C., 1991, *MNRAS*, 252, 414 (ES)
 Evrard, A. E. & Henry, J. P., 1991, *ApJ*, 383, 95 (EH)
 Frenk, C. S., White, S. D. M., Efstathiou, G., Davis, M., 1990 *ApJ*, 351, 10
 Henry J. P., Gioia I. M., Maccacaro T., Morris S. L., Stocke J. T., Wolter A., 1992, *ApJ*, 386, 408
 Holden et al., 1997, *ApJ*, submitted
 Kaiser, N., 1986, *MNRAS*, 222, 232
 Kaiser, N., 1991, *ApJ*, 383, 104
 Kauffmann, G., 1995, preprint
 Kendall, M. G. & Stewart, A., 1973, *The Advanced Theory of Statistics*, Hafner: New York
 Lynden-Bell, D., 1967, *MNRAS*, 136, 101
 Melnick, J., 1991, EFOSC1 Update to the Operating Manual, ESO Publications
 Merritt, D., 1987, *ApJ*, 313, 121
 Merritt, D. & Tremblay, A. J., 1994, *AJ*, 108, 514
 Nichol, R. C., Ulmer, M. P., Kron, R. G., Wirth, G. B., Koo, D. C., 1994, *ApJ*, 432, 464
 Nichol, R. C., Holden, B. P., Romer, A. K., Ulmer, M. P., Burke, D. J., Collins, C. A., 1997, *ApJ*, in press.
 Padmanabhan, T., 1993, *Structure Formation in the Universe*, Cambridge University Press
 Rosati, P., Della Ceca, R., Burg, R., Norman, C., Giacconi, R., 1995, *ApJ*, 445, 11
 Zabludoff, A. I., Huchra, J. P., Geller, M.J., 1990, *ApJS*, 74, 1
 Zabludoff, A. I., Geller, M.J., Huchra, J. P., Ramella, M., 1993, *AJ*, 106, 1301

FINDING CHARTS

A compressed tar file containing the full set of finding charts can be obtained from <http://star-www.dur.ac.uk/~rgb/>.

Plate 1(a–g). Finding charts of the CEMM cluster fields studied in this project: (a) F1557.19TC, (b) F1652.20CR, (c) F1637.23TL, (d) J2175.15TR, (e) J2175.23C, (f) F1835.22CR, (g) F1835.2CL. Objects are labeled either by their original CEMM designation, or by the slit number with prefix A or B to distinguish the first and second masks. All the images are reproduced to the same angular scale, with the larger images giving a $5' \times 5'$ area. For $H_0 = 50 \text{ km s}^{-1} \text{ Mpc}^{-1}$ and $q_0 = 0.5$, this corresponds to a $2 \times 2 \text{ Mpc}^2$ region at $z = 0.41$. Our spectroscopy concentrated on objects close to the cluster center, however: almost all cluster members come from within the central 0.5 Mpc. With the exception of Plate 1f (F1835.22CR), the field is oriented with North up and East to the left; Plate 1f is rotated by 45° so that the top right-hand corner points North.

This paper has been produced using the Royal Astronomical Society/Blackwell Science \TeX macros.